Materials Letters 161 (2015) 735–739

Contents lists available at ScienceDirect

Materials Letters

journal homepage: www.elsevier.com/locate/matlet

Amorphization of crystalline phases in the Nd–Fe–B alloy driven by the high-pressure torsion

B.B. Straumal [a,b,c,*], A.A. Mazilkin [a,b], S.G. Protasova [a,b], D.V. Gunderov [c], G.A. López [c,d], B. Baretzky [b,c]

[a] Institute of Solid State Physics, Russian Academy of Sciences, Chernogolovka, Russia
[b] Karlsruher Institut für Technologie, Institut für Nanotechnologie, Eggenstein-Leopoldshafen, Germany
[c] Laboratory of Hybrid Nanomaterials, National University of Science and Technology, MISIS, Moscow, Russia
[d] Applied Physics II, University of the Basque Country UPV-EHU, Bilbao, Spain

ARTICLE INFO

Article history:
Received 6 September 2015
Accepted 14 September 2015
Available online 16 September 2015

Keywords:
Phase transitions
Severe plastic deformation
Amorphization
Permanent magnets

ABSTRACT

High pressure torsion (HPT) has been used for the severe plastic deformation (SPD) treatment of molten Fe–12.3 at% Nd–7.6 at% B alloy (5 GPa, 1 rpm, 5 rot, room temperature). After HPT the microstructure contained the nanograins of the ferromagnetic $Nd_2Fe_{14}B$ phase embedded in the amorphous matrix with uniform composition. It is different to the commercial multicomponent FeNdB-based alloy where two different amorphous phases appeared after HPT (B.B. Straumal, A.R. Kilmametov, A.A. Mazilkin, S.G. Protasova, K.I. Kolesnikova, P.B. Straumal, B. Baretzky, Mater. Lett., 2015, 145, pp. 63–66). The SPD-treatment at room temperature $T_{SPD}=30$ °C is frequently equivalent to the heat treatment at a certain elevated temperature $T_{eff}>30$ °C. The composition of phases in the studied NdFeB-based alloy after HPT corresponds to the state at $T_{eff}\sim1140$ °C.

1. Introduction

Nowadays, about 30 years after their discovery, NdFeB-based alloys remain the best materials for permanent magnets [1]. It is because of their high spontaneous polarization J_S, crystalline anisotropy K_1 and Curie-temperature T_C ($J_S>1.2$ T, $K_1>10^6$ J/m^3, $T_C>250$ °C). These properties ensure the high value of their energy product $(BH)_{max}>450$ kJ/m^3 [2]. Nevertheless, the further development of these materials is very important [3]. The best magnetic properties of NdFeB-based alloys can be reached when the fine grains of the ferromagnetic $Nd_2Fe_{14}B$ phase are separated by the thin layers of a non-magnetic phase [3]. The NdFeB-based permanent magnets are mainly manufactured using liquid phase sintering of magnetically oriented powders [4]. The alternative manufacture route starts with a melt spinning which permits to obtain the nanocrystals embedded in the amorphous phase or contacting each other [5].

However, the development of principally new methods for the production of NdFeB-based permanent magnets is extremely important. One of such methods is the severe plastic deformation (SPD) [6]. The SPD permits to increase the strain up to enormous values without fracture of a material, because the material is strained in a confined space. SPD frequently leads to various phase transformations in the materials [7–11]. In other words, the phases before and after SPD are different. Thus, SPD can induce the dissolution of phases [12,13], formation [14,15] or decomposition [16,17] of a supersaturated solid solution, disordering of ordered phases [18], amorphization of crystalline phases [19,20], synthesis of the low-temperature [21], high-temperature [22] or high-pressure [23–26] allotropic modifications of metals, formation of intermetallic compounds [27], and nanocrystallization in the amorphous matrix [28]. In many systems the phases appearing after SPD frequently are the same as those existing after an annealing at a certain (mostly elevated) temperature [11,15,17,25,27]. This temperature is the so-called effective temperature T_{eff}. In the case of NdFeB-based alloys SPD has been used in several works to obtain the desired properties [29–40]. The fine-grained or even nanograined microstructure has been formed after SPD of as-cast samples [29,30,39,40] or nanocrystallization took place in the amorphous matrix after SPD of melt-spun alloys [31–38]. The direct amorphization of an as-cast crystalline NdFeB alloy under high pressure torsion (HPT) was analyzed in the present work and the results were compared with those obtained after HPT of a commercial liquid-phase sintered multicomponent NdFeB-based

* Corresponding author at: Institute of Solid State Physics, Russian Academy of Sciences, Chernogolovka, Moscow District, 142432, Russia. Fax: +7 499 2382326.
E-mail address: straumal@issp.ac.ru (B.B. Straumal).

http://dx.doi.org/10.1016/j.matlet.2015.09.076
0167-577X/

alloy [40]. In latter case the HPT had driven the formation of a mixture of two different amorphous phases with embedded grains of the ferromagnetic $Nd_2Fe_{14}B$ phase [40]. In the current case only one amorphous phases with embedded $Nd_2Fe_{14}B$ grains appears after HPT.

2. Experimental

The Fe–12.3 at% Nd–7.6 at% B alloy was investigated. This composition is close to that of the most important magnetic compound $Fe_{14}Nd_2B$ (*T*-phase) in the Fe–Nd–B system (Fig. 1) [41–43]. This alloy has been investigated previously in order to characterize the wetting of $Fe_{14}Nd_2B/Fe_{14}Nd_2B$ grain boundaries by the Nd-rich melt [44,45]. The alloy was prepared from high purity components (5N Fe, 4N Nd and 4N B) by vacuum induction melting. For HPT processing, the 0.6 mm thick discs were cut from the as-cast ingots, then ground and chemically etched. The disks were subjected to HPT in a Bridgman anvil type unit (room temperature, pressure 5 GPa, 5 torsions, 1 rpm) using a custom built HPT device [29,33,34,36,38,39]. After HPT, the central (low-deformed) part of each disk (about 3 mm in diameter) was excluded from further investigations. The samples for structural investigations were cut from the deformed disks at a distance of 4–5 mm from the sample centre. Transmission electron microscopy (TEM, HRTEM, STEM, EDXS) studies were carried out on the TECNAI instrument. X-ray diffraction (XRD) data were obtained on a Siemens diffractometer (Co Kα radiation). The magnetic properties were measured on a superconducting quantum interference device SQUID (Quantum Design MPMS-7 and MPMS-XL).

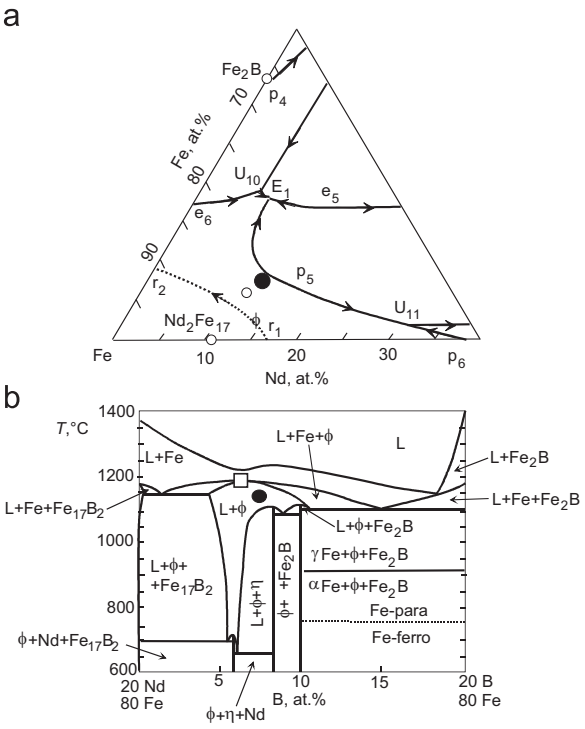

Fig. 1. (a) Liquidus projection close to the Fe-corner of the Fe–Nd–B phase diagram [41–43]. Open circles mark the Fe_2B, Nd_2Fe_{17} and $Fe_{14}Nd_2B$ (φ) binary and ternary compounds. The composition of the investigated alloy is shown by the solid circle. E_1 is the ternary eutectic point $L=\gamma Fe+Fe_{14}Nd_2B+Fe_7Nd_2B_6$ at 1090 °C. e_5 is the eutectic point $L=Fe_{14}Nd_2B+Fe_7Nd_2B_6$ (η) at 1095 °C. e_6 is the eutectic point $L=\gamma Fe+Fe_2B$ at 1177 °C. U_{10} is the transformation $L+Fe_2B=\gamma Fe+Fe_7Nd_2B_6$ (η). U_{11} is the transformation $L+\gamma Fe=Nd_2Fe_{17}+Fe_{14}Nd_2B$. p_4 is the peritectic point $L+FeB=Fe_2B$ at 1407 °C. p_5 is the peritectic point $L+\gamma Fe=Fe_{14}Nd_2B$ at 1407 °C. p_6 is the peritectic point $L+\gamma Fe=Fe_{17}Nd_2$ at 1185 °C. r_1 is the remelting point $\delta Fe=L+\gamma Fe$ at 1392 °C. r_3 is the remelting point $\delta Fe=L+\gamma Fe$ at 1381 °C. (b)The 80 at% Fe section of the Fe–Nd–B phase diagram [41–43]. Large filled circle shows the effective temperature $T_{eff}=1140\pm30$ °C in the $L+\varphi$ area (one liquid phase→one amorphous phase). Large open square shows the effective temperature $T_{eff}=1170\pm30$ °C obtained for the commercial Fe–Nd–B alloy [40]. Large open circle is on the border between $L+\varphi$ and $L+Fe$ areas (two liquid phases→two amorphous phases, Fe-rich and Nd-rich).

3. Results and discussion

The torsion torque in the NdFeB-based alloy becomes stationary after about 2.5 anvil rotations. After quick starting increase of torsion torque from zero to ~250 N m, the slow work hardening takes place. The torsion torque linearly increases till ~2.5 anvil rotations. After this point the torsion torque stabilizes around 400 N m. The molten as-cast sample contained the mixture of major $Nd_2Fe_{14}B$ phase (*T*-phase) and minor crystalline Nd-rich solid solution (Fig. 2a) with grain size about 200–300 μm [44,45]. The initial molten as-cast alloys amorphizes during HPT (Fig. 2b). XRD pattern in Fig. 2b clearly shows the amorphous halo and broad peaks of crystalline $Nd_2Fe_{14}B$ phase. HREM images and FFT-patterns (Fig. 2c) show that HPT-treated samples contain the amorphous phase with spatially uniform composition with embedded $Nd_2Fe_{14}B$ (*T*-phase) nanograins with size of 10–20 nm. The HPT leads also to the strong improvement of the magnetic properties in comparison with molten alloy. For example, the coercivity H_c increases about 15 times from 0.025 (Fig. 3a) to 0.38 T (Fig. 3b). This is mainly due to the strong grain refinement.

In our previous work [40] we observed that HPT (under the same conditions) of a multicomponent commercial liquid-phase sintered NdFeB-based alloy also led to the amorphization and formation of nanograins in the $Nd_2Fe_{14}B$ amorphous matrix. However, the amorphous matrix contained areas of two different phases, namely Nd-rich and Fe-rich. The HAADF STEM images witnessed the light (Nd-rich) and dark (Fe-rich) areas with concentration steps in line-scans across the border between them. In the FFT from the HREM images two different amorphous halos from the Nd-rich and Fe-rich areas were clearly visible. Nothing similar to these phenomena was observed after HPT for the ternary FeNdB alloys investigated in the present work.

Thus, the strong external forces acting during HPT caused the phase transformation in the material, namely the formation of the amorphous phase from crystalline ones and very strong refinement of $Nd_2Fe_{14}B$ grains. Historically, such unusual behavior as amorphisation of crystalline phases without quenching from the melt was first observed in materials under severe irradiation [46]. Only much later it has been observed that the transformation from crystalline state to an amorphous one under SPD can take place as a result of a solid-state reaction at the room temperature [47,48]. Based on these experimental observations, G. Martin proposed a simplified mean-field description of solid solutions subjected to irradiation-induced atomic mixing [49]. The main idea of G. Martin was that the irradiation induces the forced mixing of atoms. In turn, this mixing emulates the increase of entropy and changes the thermodynamic potentials in the alloy. G. Martin also for the first time proposed the idea to use the equilibrium phase diagram for the description of the system under irradiation. He saw that the phases that appeared after irradiation at room temperature T_{irr} can be found in the equilibrium phase diagram at a certain elevated effective temperature T_{eff}. Consequently, the irradiation can drive the dissolution of precipitates of a second phase and to the formation of supersaturated solid solutions. Or, if the liquid phase is present in the phase diagram at the T_{eff}, an amorphous phase would appear under irradiation [49,50].

In our case, the composition of the phases after SPD allows to localize them in the corresponding equilibrium phase diagram (as already done previously for the Cu-, Al-, Ti- or Zr-based alloys

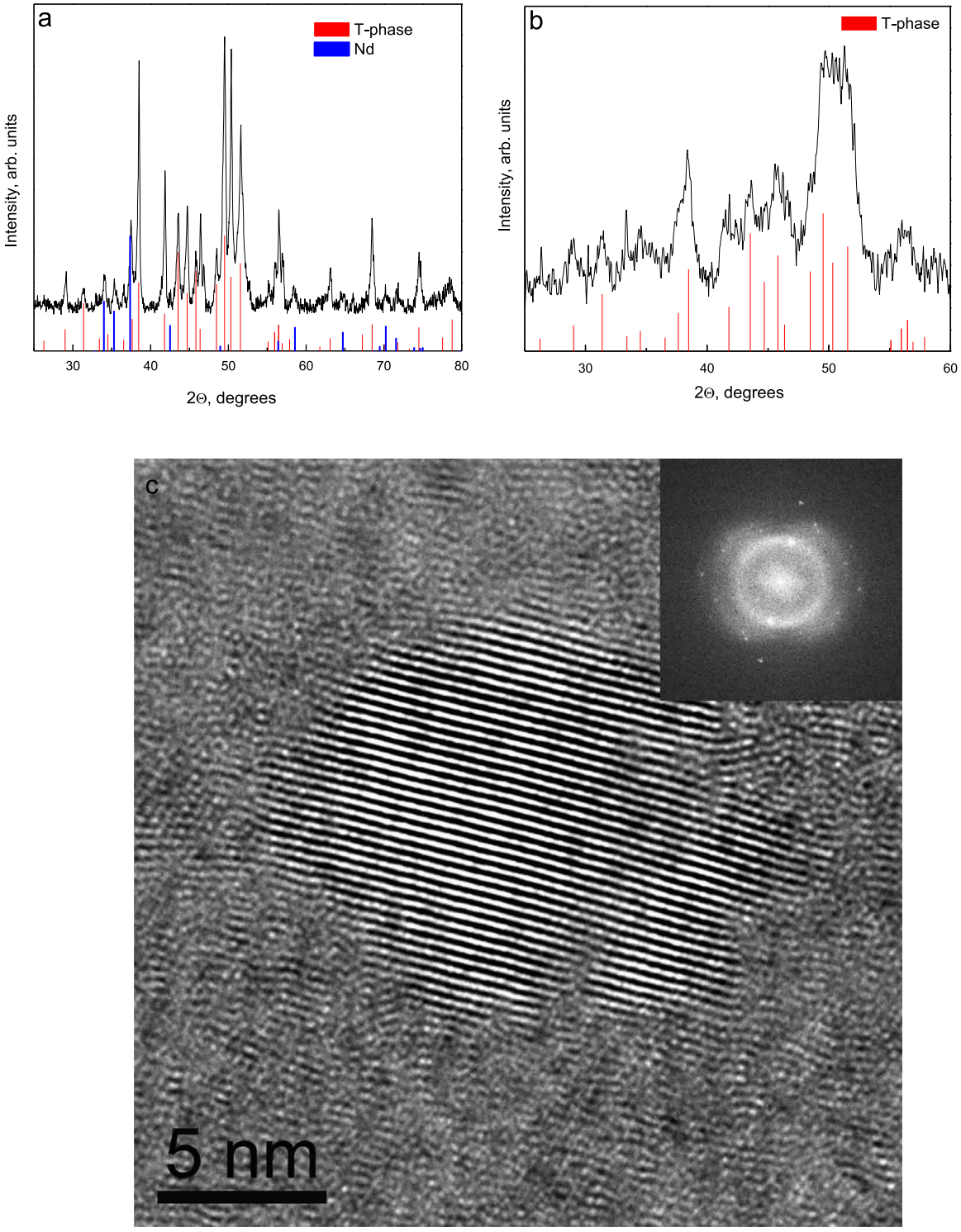

Fig. 2. (a, b) XRD patterns of the Nd–Fe–B alloy (a) as-cast (b) after HPT. The amorphous halo is visible under the main wide peak. The positions of the reflections from $Nd_2Fe_{14}B$ phase (*T*-phase) are indicated by thin vertical lines. The positions of the reflections from Nd phase are indicated by thick vertical lines. (c) HREM image of the sample after HPT and PPT-pattern (inset). $Nd_2Fe_{14}B$ phase nanocrystal is visible in the middle of the image. It is surrounded by the amorphous matrix of uniform composition. (For interpretation of the references to color in this figure legend, the reader is referred to the web version of this article.)

[10,11,25,27]) and to estimate the effective temperature T_{eff}. In our previous work the application of HPT to a multicomponent commercial liquid-phase sintered NdFeB-based alloy led to the formation of two amorphous phases [40]. Such state is shown in the Nd–Fe–B phase diagram (Fig. 1b) by the open square on the border between $L+\varphi$ and $L+$Fe areas, where two liquid phases of different composition are present. Therefore, the effective temperature in [40] was slightly above 1150 °C and could be estimated as $T_{eff}=1170\pm30$ °C. The formation of the mixture of two different amorphous phases from crystalline ones under the action of HPT has been observed for the first time in Ni–Nb–Y alloys [51]. In the Ni–Nb–Y alloys the regions of two different amorphous phases were very fine (few nm) and uniformly mixed. In this work only one amorphous phase is present after HPT surrounding the

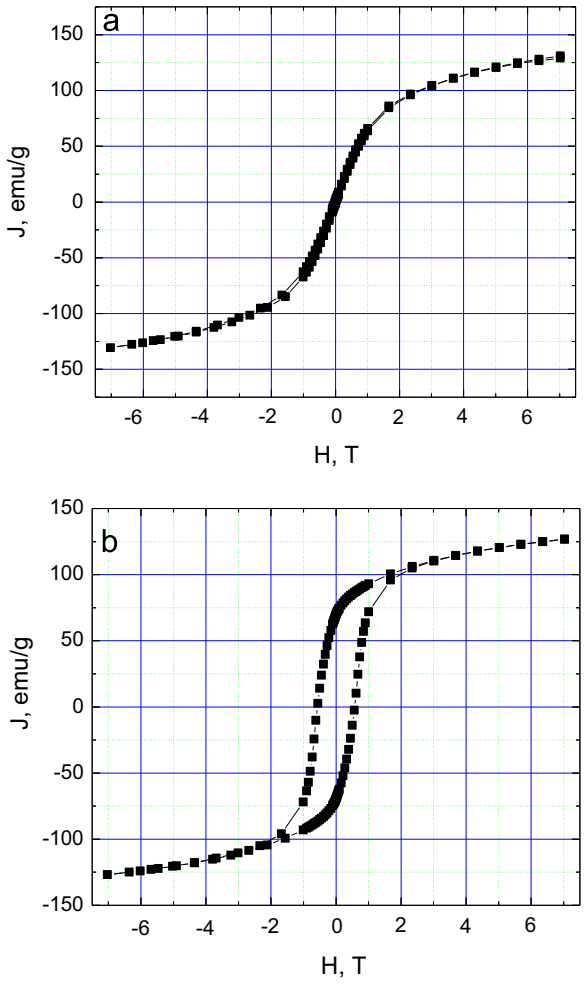

Fig. 3. Dependence of magnetization J on the applied magnetic field H before (a) and after (b) HPT.

nanograins of φ-phase (Fig. 2). This is equivalent to the $L+\varphi$ area of the Nd–Fe–B equilibrium phase diagram and is shown by the solid circle. As conclusion, the pertinent effective temperature can be estimated as $T_{\text{eff}}=1140\pm30$ °C.

4. Conclusions

Severe plastic deformation by HPT leads to the phase transitions and strong grain refinement in several metallic alloys. After HPT of an as-cast Fe–12.3 at% Nd–7.6 at% B alloy the microstructure contained the nanograins of the ferromagnetic $Nd_2Fe_{14}B$ phase embedded in an amorphous matrix with uniform composition. The resulting microstructure is different to that obtained for a commercial multicomponent FeNdB-based alloy where two different amorphous phases were formed after HPT [40]. SPD-treatment at room temperature T_{SPD} is frequently equivalent to the heat treatment at a certain elevated (effective) temperature T_{eff}. According to the composition of the phases observed in the studied NdFeB-based alloy, after HPT the relevant effective temperature $T_{\text{eff}}\sim1140$ °C.

Acknowledgments

The work was partially supported by the Russian Foundation for Basic Research (Grants 15-03-01127, 14-48-03598 and 14-42-03621), Government of Moscow Region (grant 14-48-03598), Ministry of Education and Science of the Russian Federation in the framework of Increase Competitiveness Program of MISiS (Grant К2-2014-013) and for the Grant 14.A12.31.0001, Karlsruhe Nano Micro Facility, and the Allianz Industrie Forschung (Grant FE.5150.0028.4067).

References

[1] T. Schrefl, J. Fidler, H. Kronmüller, Phys. Rev. B 49 (1994) 6100–6110.
[2] W. Rodewald, Rare-earth transition-metal magnets, in: H. Kronmüller, S. Parkin (Eds.), Handbook of Magnetism and Advanced Magnetic Materials, John Wiley & Sons, Hoboken, 2007, pp. 1969–2004.
[3] D. Goll, R. Loeffler, J. Herbst, R. Karimi, G. Schneider, J. Phys. Condens. Matter 26 (2014) 064208.
[4] J.F. Herbst, Rev. Mod. Phys. 63 (1991) 819–898.
[5] A. Manaf, R.A. Buckley, H.A. Davies, J. Magn. Magn. Mater. 128 (1993) 302–306.
[6] R.Z. Valiev, R.K. Islamgaliev, I.V. Alexandrov, Prog. Mater. Sci. 45 (2000) 103–189.
[7] E.I. Teitel', L.S. Metlov, D.V. Gunderov, A.V. Korznikov, Phys. Metall. Metallogr. 113 (2012) 1162–1168.
[8] X. Sauvage, A. Chbihi, X. Quelennec, J. Phys. Conf. Ser. 240 (2010) 012003.
[9] B.B. Straumal, X. Sauvage, B. Baretzky, A.A. Mazilkin, R.Z. Valiev, Scr. Mater. 70 (2014) 59–62.
[10] B. Straumal, A. Korneva, P. Zięba, Arch. Civil Mech. Eng. 14 (2014) 242–249.
[11] B.B. Straumal, A.R. Kilmametov, Ivanisenko Yu, A.A. Mazilkin, O.A. Kogtenkova, L. Kurmanaeva, A. Korneva, P. Zięba, B. Baretzky, Int. J. Mater. Res. 106 (2015) 657–664.
[12] B.B. Straumal, S.V. Dobatkin, A.O. Rodin, S.G. Protasova, A.A. Mazilkin, D. Goll, B. Baretzky, Adv. Eng. Mater. 13 (2011) 463–469.
[13] X. Sauvage, Y. Ivanisenko, J. Mater. Sci. 42 (2007) 1615–1621.
[14] X. Sauvage, P. Jessner, F. Vurpillot, R. Pippan, Scr. Mater. 58 (2008) 1125–1128.
[15] B.B. Straumal, A.R. Kilmametov, A.A. Mazilkin, L. Kurmanaeva, Y. Ivanisenko, A. Korneva, P. Zięba, B. Baretzky, Mater. Lett. 138 (2015) 255–258.
[16] B.B. Straumal, B. Baretzky, A.A. Mazilkin, F. Phillipp, O.A. Kogtenkova, M. N. Volkov, R.Z. Valiev, Acta Mater. 52 (2004) 4469–4478.
[17] B.B. Straumal, S.G. Protasova, A.A. Mazilkin, E. Rabkin, D. Goll, G. Schütz, B. Baretzky, R. Valiev, J. Mater. Sci. 47 (2012) 360–367.
[18] A.V. Korznikov, G. Tram, O. Dimitrov, G.F. Korznikova, S.R. Idrisova, Z. Pakiela, Acta Mater. 49 (2001) 663–671.
[19] S.D. Prokoshkin, Khmelevskaya IYu, S.V. Dobatkin, I.B. Trubitsyna, E. V. Tatyanin, V.V. Stolyarov, et al., Acta Mater. 53 (2005) 2703–2714.
[20] X. Sauvage, L. Renaud, B. Deconihout, D. Blavette, D.H. Ping, K. Hono, Acta Mater. 49 (2001) 389–394.
[21] V.V. Sagaradze, V.A. Shabashov, Nanostruct. Mater. 9 (1997) 681–684.
[22] MacLaren I. IvanisenkoYu, X. Sauvage, R.Z. Valiev, H.-J. Fecht, Acta Mater. 54 (2006) 1659–1669.
[23] M.T. Pérez-Prado, A.P. Zhilyaev, Phys. Rev. Lett. 102 (2009) 175504.
[24] Ivanisenko Yu, A. Kilmametov, H. Rösner, R.Z. Valiev, Int. J. Mater. Res. 1 (2008) 36–41.
[25] B.B. Straumal, A.R. Kilmametov, Ivanisenko Yu, A.S. Gornakova, A.A. Mazilkin, M.J. Kriegel, O.B. Fabrichnaya, B. Baretzky, H. Hahn, Adv. Eng. Mater. 17 (2015) 10.1002/adem.201500143.
[26] B.B. Straumal, A.S. Gornakova, A.A. Mazilkin, O.B. Fabrichnaya, M.J. Kriegel, B. Baretzky, J.-Z. Jiang, S.V. Dobatkin, Mater. Lett. 81 (2012) 225–228.
[27] B.B. Straumal, A.R. Kilmametov, Kucheev YuO, K.I. Kolesnikova, A. Korneva, P. Zięba, B. Baretzky, JETP Lett. 100 (2014) 376–379.
[28] P. Henitz, Zs. Kovacs, A.P. Zhilyaev, Á. Révész, Scr. Mater. 54 (2006) 1733–1737.
[29] V.V. Stolyarov, D.V. Gunderov, A.G. Popov, T.Z. Puzanova, G.I. Raab, A.R. Yavari, J. Magn. Magn. Mater. 242 (2002) 1399–1401.
[30] A.G. Popov, V.S. Gaviko, N.N. Shchegoleva, T.Z. Puzanova, A.S. Ermolenko, V. V. Stolyarov, Phys. Metall. Metallogr. 94 (2002) S75–S81.
[31] H.L. Li, L. Lou, F.C. Hou, D.F. Guo, W. Li, X.H. Li, Appl. Phys. Lett. 14 (2013) 142406.
[32] A.G. Popov, V.V. Serikov, N.M. Kleinerman, Phys. Metall. Metallogr. 109 (2010) 505–513.
[33] W. Li, D.F. Guo, X.H. Li, Y. Chen, D.V. Gunderov, V.V. Stolyarov, J. Appl. Phys. 108 (2010) 053901.
[34] W. Li, X.H. Li, D.F. Guo, K. Sato, D.V. Gunderov, V.V. Stolyarov, Appl. Phys. Lett. 94 (2009) 231904.
[35] W. Li, L.L. Li, Y. Nan, Z.Y. Xu, X.Y. Zhang, A.G. Popov, J. Appl. Phys. 104 (2008) 023912.
[36] A.G. Popov, V.S. Gaviko, N.N. Shchegoleva, L.A. Shreder, V.V. Stolyarov, D. V. Gunderov, Phys. Metall. Metallogr. 104 (2007) 238–247.
[37] W. Li, L.L. Li, Y. Nan, X.H. Li, X.Y. Zhang, Appl. Phys. Lett. 91 (2007) 062509.
[38] A.G. Popov, V.S. Gaviko, N.N. Shchegoleva, L.A. Shreder, D.V. Gunderov, V. V. Stolyarov, J. Iron Steel Res. Int. 13 (2006) 160–165.
[39] H. Li, L. Lou, F. Hou, D. Guo, W. Li, X. Li, D.V. Gunderov, K. Sato, X. Zhang, Appl. Phys. Lett. 103 (2013) 142406.
[40] B.B. Straumal, A.R. Kilmametov, A.A. Mazilkin, S.G. Protasova, K.I. Kolesnikova, P.B. Straumal, B. Baretzky, Mater. Lett. 145 (2015) 63–66.
[41] Z.S. Ji, M.L. Hu, X.P. Zheng, J. Mater. Sci. Technol. 23 (2007) 247–252.

[42] Y.A. Shatilla, E.P. Loewen, Nucl. Technol. 151 (2005) 239–249.
[43] M. Sagawa, S. Fujimura, N. Togawa, H. Yamamoto, Y. Matsuura, J. Appl. Phys. 55 (1984) 2083–2087.
[44] B.B. Straumal, Yu.O. Kucheev, I.L. Yatskovskaya, I.V. Mogilnikova, G. Schütz, B. Baretzky, J. Mater. Sci. 47 (2012) 8352–8359.
[45] Yu.O. Kucheev, A.B. Straumal, I.V. Mogil'nikova, B.B. Straumal, A.M. Gusak, B. Baretzky, Russ. J. Non-Ferr. Met. 53 (2012) 450–456.
[46] X. Sauvage, G. Wilde, S.V. Divinski, Z. Horita, R.Z. Valiev, Mater. Sci. Eng. A 540 (2012) 1–12.
[47] R.V. Sundeev, A.M. Glezer, A.V. Shalimova, Mater. Lett. 133 (2014) 32–34.
[48] R.V. Sundeev, A.M. Glezer, A.V. Shalimova, J. Alloy. Compd. 611 (2014) 292–296.
[49] G. Martin, Phys. Rev. B 30 (1984) 1424–1436.
[50] G. Thomas, H. Mori, H. Fujita, Scr. Metall. 16 (1982) 589–592.
[51] A.A. Mazilkin, G.E. Abrosimova, S.G. Protasova, B.B. Straumal, G. Schütz, S. V. Dobatkin, A.S. Bakai, J. Mater. Sci. 46 (2011) 4336–4342.